Available online www.jocpr.com

Journal of Chemical and Pharmaceutical Research, 2012, 4(6):2937-2951

Research Article

ISSN : 0975-7384
CODEN(USA) : JCPRC5

Molecular determinants of ligand binding at the human histamine H_1 receptor: Site-directed mutagenesis results analyzed with ligand docking and molecular dynamics studies at H_1 homology and crystal structure models.

Tania C. Cordova-Sintjago [1,*], Lijuan Fang [1], Martijn Bruysters [2], Rob Leurs [2], Raymond G. Booth [1, 3]

[1]Department of Medicinal Chemistry, University of Florida, Gainesville, Florida 32610 US
[2]Department of Pharmacochemistry, Vrije Universiteit, Amsterdam, the Netherland
[3]Northeastern University Center for Drug Discovery, Boston, Massachusetts 02115, USA

ABSTRACT

The human histamine H_1 G-protein coupled receptor (GPCR) is an important drug target for inflammatory, sleep, and other neuropsychiatric disorders. To delineate molecular determinants for ligand binding for drug discovery purposes, human H_1 receptor models were built by homology to the crystal structure of the human β_2 adrenoceptor (β_2AR) and from the recently reported crystal structure of the human H_1 receptor complex with doxepin at 3.1 Å (PDB code 3RZE). Ligand affinity of histamine and the H_1 antagonists mepyramine and (2S, 4R)-(–)-trans-4-phenyl-2-N, N-dimethylaminotetralin (PAT) at wild type and point-mutated (D3.32A, Y3.33A, W4.56A, F5.47A, W6.48A, Y6.51A, F6.52A, F6.55A, Y7.43A) human H_1 receptors were determined experimentally and results analyzed by ligand docking and molecular dynamic studies at WT and point-mutated H_1 receptor models. Differences in ligand binding affinities correlated to differences in ligand binding modes at models built according to homology or crystal structure, indicating, both models are accurate templates for predicting ligand affinity for H_1 drug design.

Keywords: Human histamine H1 G protein-coupled receptor (GPCR), homology modeling, docking, molecular dynamics, site-directed mutagenesis

---

INTRODUCTION

Histamine mediates its numerous physiological functions via activation of H_1, H_2, H_3, and H_4 G-protein coupled receptors (GPCRs) [1]. The human histamine H_1 GPCR is expressed in various tissues, including, bronchial, intestinal, and vascular smooth muscle, as well as, brain [2]. Thus, in addition to the well-known success of targeting the H_1 receptor for allergy and other inflammatory diseases [2], the H_1 receptor also is a drug target for sleep disorders and other neurodegenerative and neuropsychiatric diseases [1, 3].

GPCRs are membrane proteins that share a 3-dimensional structure consisting of a bundle of seven transmembrane (TM) alpha helices, connected by alternating intracellular and extracellular loops, with the N-terminus in the extracellular domain and C-terminus in the intracellular domain. Several GPCR crystal structures have been reported, including, bovine rhodopsin (bRho) [4-8], opsin, [9,10], human A_{2A} adenosine receptor (AA_2AR) [11], turkey β_1 adrenoceptor (β_1AR) [12], human β_2 adrenoceptor (β_2AR) in an inactive state [13-16], β_2AR in a

nanobody-stabilized active-state [17], and β_2AR in complex with an irreversible agonist [18, 19], human dopamine D_3 receptor in complex with an agonist [20]. Recently, the crystal structure of the human H_1 receptor in a complex with the H_1 inverse agonist/antagonist doxepin at 3.1 Å (PDB code 3RZE) was reported [21].

Essentially all ligands for monoaminergic neurotransmitter (dopamine, histamine, norepinephrine/noradrenalin, serotonin) GPCRs contain a basic amine moiety. The endogenous neurotransmitters have a primary amine moiety, but, ligands with secondary or tertiary amine groups also are common [22, 23]. Mutagenesis studies indicate that the fully-conserved aspartate residue D3.32 of monoaminergic neurotransmitter GPCRs interacts with the positively charged amine moiety of endogenous agonists and other ligands at physiological pH, and this ionic interaction is critical for ligand binding [24-26]. For example, we recently reported that mutation of D3.32 to alanine (D3.32A) in the serotonin (5-hydroxytryptamine, 5-HT) 5-HT_{2C} GPCR abolishes detectable binding of the standard 5-HT_{2C} radioligand [^{3}H]-mesulergine [27]. Often, such experimental data from mutagenesis studies is used to validate GPCR receptor models and ligand docking studies. Thus, in the absence of a 5-HT_{2C}, crystal structure, we recently reported ligand docking and molecular dynamics results using a 5-HT_{2C} receptor model built by homology to the human β_2AR [27, 28] and validated by experimental affinity data using the wild type (WT) and point-mutated 5-HT_{2C} receptors [28].

In this work, we report affinity for ligand binding at the WT and point-mutated (D3.32A, Y3.33A, W4.56A, F5.47A, W6.48A, Y6.51A, F6.52A, F6.55A, Y7.43A) human H_1 receptors. Ligands studied include the endogenous agonist histamine, as well as, mepyramine and (2*S*, 4*R*)-(–)-*trans*-4-phenyl-2-*N*, *N*-dimethylaminotetralin -(2*S*, 4*R*)-PAT, both, antagonists regarding H_1-mediated activation of phospholipase C signaling [29]. Experimental binding affinity results are interpreted in light of results of ligand docking and molecular dynamics (MD) studies carried out at models of the WT and point-mutated H_1 receptors built by homology to the structure of the β_2AR/T4-lysozyme chimera (Protein Data bank entry 2RH1) [15] and from the recently reported crystal structure of the human H_1 receptor in a complex with the H_1 antagonist ligand doxepin at 3.1 Å (PDB code 3RZE) [21]. In addition, we compare the β_2AR-based H_1 homology and 3RZE crystal structure models reported here to a previously reported bRho-based H_1 homology model [26] and discuss the implications for GPCR homology modeling in drug discovery and development.

EXPERIMENTAL SECTION

Human H_1 receptor model building and molecular dynamics simulations

The homology model of the human H_1 GPCR was built based on the crystal structure of the β_2AR/T4-lysozyme chimera (Protein Data bank entry 2RH1) [15]. The human H_1 native sequence was aligned to the β_2AR sequence using *ClustalW* multiple sequence alignment [30, 31]. Point mutations were performed as needed and the gaps were analyzed, followed by the appropriate sequence additions and deletions to match the human H_1 receptor amino acid sequence. The TM domains were built using the Biopolymer module of *Sybyl 8.1* [32]. The inverse agonist carazolol, present in the crystal structure of the human hβ_2AR (2RH1), was deleted and the resulting 7-TM bundle was optimized using Tripos force field [33]. Regions outside the 7-TM bundle such as the human H_1 N-terminus, C-terminus, extracellular and intracellular loop residues were built using loop database PRODAT in *Sybyl* 8.1. The crude model was minimized using the Powell method implemented in *Sybyl* with Tripos force field [33] and AMBER charges [34]. The resulting model was inserted into a rectangular box containing a pre-equilibrated 1-palmitoyl-2-oleyl-*sn*-glycero phosphatidyl choline (POPC) bilayer [35] that consisted of 200 lipid molecules, forming a rectangular patch, and 5,483 water molecules covering the head groups on each side of the bilayer. The system containing the WT human H_1 receptor model within the simulated membrane contained 47,495 atoms. The system was relaxed using the Tripos force field to a gradient 0.05 kcal/mol Å, prior to molecular dynamics (MD) simulation in the POPC membrane.

MD simulation conditions were time run 10 ns, time step 1 fs, with snapshots collected every 5 fs. Simulations were carried out using the canonical ensemble NVT (constant number of particles, volume and temperature) at 300K temperature, Boltzmann initial velocities, and non-bonded cutoff set at 8 Å. Constraints for alpha carbons in the TM domains were employed. Subsequently, the constraints were removed for a 2 ns MD simulation run. The final H_1 homology model was obtained from the median structure after clustering analyses of the frames from the last 10 ns of the MD simulation, and optimized using the Tripos force field to a convergence of 0.05 Kcal/mol Å.

A WT H_1 receptor model also was built based on the crystal structure of the human H_1 receptor in a complex with the H_1 antagonist doxepin (PDB code 3RZE, [21]. After removing doxepin, the structure was equilibrated using MD simulations, as described above.

The homology models of the D3.32A, Y3.33A, W4.56A, F5.47A, W6.48A, Y6.51A, F6.52A, F6.55A, and Y7.43A point-mutated human H_1 receptors were built by point mutations of the β_2AR-bassed WT H_1 homology model; relaxation and MD procedures were as described above.

Ligand docking.
In addition to the endogenous agonist histamine, the H_1 ligands used in this study were mepyramine and (2*S*, 4*R*)-PAT (Figure 1), both, antagonist ligands regarding H_1-mediated activation of PLC signaling, and both available as tritiated radioligands that allow for direct measurement of their binding affinity [23,29,36]. The ligand structures were built as monocations (protonated amines) using *HyperChem 8.0* [37] and structures were optimized using PM3 model Hamiltonian to a gradient of 0.01 Kcal/mol Å.

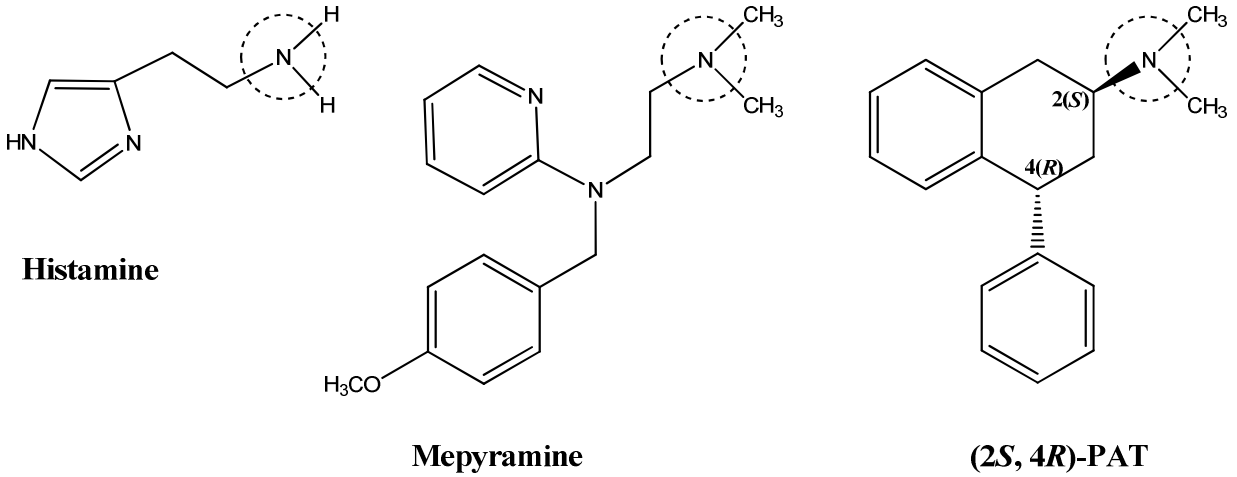

Figure 1. Ligands used in H_1 docking studies; circled is the amine function that is protonated at physiological pH.

Docking studies were carried out at the β_2AR-based H_1 homology model and the 3RZE crystal structure model. Ligands were pre-positioned in the binding pocket by performing rigid docking with th*e PatchDock* server [38]. The low-energy, high-score solutions were analyzed to select the initial configuration, ensuring the essential interaction between the a carboxylate oxygen of H_1 residue D3.32 and the ligand protonated amine moiety (see Figure 1) [24, 25], followed by flexible ligand docking performed with *Flexidock* in *Sybyl* 8.1. *Flexidock* uses an algorithm to probe the conformational space defining possible interactions between the ligand and its putative binding site. The binding site was defined by assigning residue D3.32 as a definitive interaction point, and including residues within a 7 Å radius. Structure preparation was carried out prior to docking studies assigning AMBER [34] charges for the protein and Gasteiger-Marsili [39] charges for the ligand. Rotatable bonds in the ligand and the side chains of residues defining the receptor putative active site were screened for optimal positioning of the ligand and side chains in the conformational space; remaining residues were frozen during docking. Default *FlexiDock* parameters were set at 80,000-generation. The best docking solution, according to the highest *FlexiDock* score, was minimized using the Tripos force field to a gradient 0.05 Kcal/mol Å, prior to molecular dynamics simulation. The selected high-score pose of the docked ligand was subjected to a MD simulation run for 5 ns with other parameters the same as above. The final structure of the ligand docked into the receptor was obtained from the average of last 10 ps of the MD simulation.

Cell culture and transfection
Human embryonic kidney 293 cells (HEK 293; from ATCC, number CRL-1573) were maintained in Eagle minimum essential medium (MEM) with 10% fetal bovine serum and 2 mM L-glutamine, 0.1 mM non-essential amino acids, 1.5 g/L sodium bicarbonate, 1.0 mM sodium pyruvate. The cDNA encoding the WT human H_1 receptor was purchased from UMR (Rolla, MO). The D3.32A, Y4.33A, W4.56A, F5.47A, W6.48A, Y6.51A,

F6.52A F6.55A, and Y7.43A point-mutated human H_1 receptors were prepared using the WT cDNA subcloned in the pAlter plasmid, according to the manufacturer's protocol (Altered Sites II, Promega). Mutations in the cDNA were verified by DNA sequencing using the dideoxy chain termination method. WT and point-mutated cDNAs were subcloned into the expression plasmid pcDEF3 [40] using the Wizard Plus Minipreps DNA purification system (Promega A7640), as previously described [27, 41, 42].

HEK cells were seeded (1-3 X 10^6 cells) in a 100 mm tissue culture dish and grown to 85-95% confluence. Cells were transfected with 24 µg of plasmid DNA using 50 µl of Lipofectamine 2000 (Invitrogen; Carlsbad, CA). Transfection continued for 24 hours, then medium was replaced with fresh growth medium without antibiotics and cells were allowed to express H_1 receptors for 24 hours. Expression of the WT and point-mutated human H_1 receptor proteins was confirmed by Western blots using an anti-histamine receptor 1 (HR1) polyclonal antibody from Chemicon (AB5654P), which was raised by an immunogen of 19 amino acid peptide sequence within the cytoplasmic loop #3 of the human H_1 receptor. For radioreceptor assays, membranes containing H_1 receptors were prepared using ice-cold 50 mM Na_2/K phosphate (Na_2HPO_4/KH_2PO_4) buffer, pH 7.4, as previously described [27, 41, 42].

Saturation and competition binding studies

Affinity (K_D) of the radioligands [^{3}H]-mepyramine (specific activity 30.0 Ci/mmol; Amersham Biosciences) and [^{3}H]-(2*S*, 4*R*)-PAT (90 Ci/mmol [28, 35]) were directly assessed in saturation binding assays using membrane preparations expressing WT or point-mutated H_1 receptors [21, 27, 41, 43]. Affinity (Ki) of histamine (Sigma-Aldrich) was assessed in competitive binding assays that measured displacement of [^{3}H]-mepyramine [26, 29, 41, 44]. K_i values were calculated by conversion of the IC_{50} data using the equation $K_i = IC_{50}/1 + L/K_D$, where L is the concentration of radioligand having affinity K_D [45]. Comparisons of affinity values between WT, D3.32A, Y3.33A, W4.56A, F5.47A, W6.48A, Y6.51A, F6.52A, F6.55A, and Y7.43A human H_1 receptors were performed using one-way analysis of variance (ANOVA) with Tukey's multiple comparison post-hoc tests.

RESULTS AND DISCUSSION

H_1 receptor homology modeling

Alignment of the native sequences of the human H_1 receptor and the template human β_2AR was carried out with *ClustalW* [30, 31]; the sequence alignment for the TM domains is shown in Table 1. Conserved residues are indicated in bold, and reference residues are labeled according to the standard Ballesteros nomenclature for GPCRs [46]. The H_1 receptor shares 34.6 % overall sequence homology with the β_2AR receptor, however, higher homology is found in TM helices (TMHs) VI and VII; 55% and 44 %, respectively. Despite the low overall sequence identity between the receptors, the TM domains contain a majority of highly conserved residues, allowing for accurate alignment.

Conserved TM domain amino acid sequences between the H_1 and β_2AR receptors were used to verify the alignment, and included the following motifs: **N**X**LVXXA** in TM I, with the reference residue N1.50; **SLX**X**ADL** in TM II, with the reference residue D2.50; **WXSXD** in TM III, with the critical reference residue D3.32; **TASI** and **DRY,** with the reference residues R3.50 in TM III and W4.50 in TM IV; **F**YX**PX**X**XM** in TM V, with the reference residue P5.50; **CW**X**PXFI** in TM VI, with the reference residues W6.48 and P6.50; **WXGYXNS** and **NPL**X**Y** in TM VII, with the reference residue P7.50.

The alignment in Table 1 was used to generate the β_2AR-based homology model of the WT human H_1 receptor. The initial model generated was optimized in vacuum and subsequently equilibrated using MD simulation in the 1-palmitoyl-2-oleyl-*sn*-glycero phosphatidyl choline (POPC) membrane, as described in the experimental section. The resulting TM bundle structure is shown in Figure 2. The overall structures of the point-mutated human H_1 receptor models (not shown) were similar to the WT human H_1 receptor (Average RMSD superposing C alphas, 0.3 Å).

Table 1 Alignment of human H_1 and β_2AR receptor sequences using *ClustalW*
Conserved residues are indicated in bold. Reference residues are labeled according to Ballesteros nomenclature [46]

	N1.50 D2.50	
ADRB2_HUMAN	NVLVITAIAKFERLQTVTNYFITSLACADLVMGLAVVPFGAAHILMKMWT	100
HRH1_HUMAN	NLLVLYAVRSERKLHTVGNLYIVSLSVADLIVGAVVMPMNILYLLMSKWS	94
	D3.32 R3.50	
ADRB2_HUMAN	FGNFWCEFWTSIDVLCVTASIETLCVIAVDRYFAITSPFKYQSLLTKNKA	150
HRH1_HUMAN	LGRPLCLFWLSMDYVASTASIFSVFILCIDRYRSVQQPLRYLKYRTKTRA	144
	W4.50 *(K5.39)*	
ADRB2_HUMAN	RVIILMVWIVSGLTSFLPIQMHWYRATHQEAINCYANETCCDFFTNQAYA	200
HRH1_HUMAN	SATILGAWFLS---FLWVIPILGWNHFMQQTSVRREDKCETDFYDVTWFK	191
	S5.43 P5.50	
ADRB2_HUMAN	IASSIVSFYVPLVIMVFVYSRVFQEAKRQLQK---IDKSEGRFHVQNLSQ	247
HRH1_HUMAN	VMTAIINFYLPTLLMLWFYAKIYKAVRQHCQHRELINRSLPSFSEIKLRP	241
	268 W6.48 Y7.43	
ADRB2_HUMAN	EHKALKTLGIIMGTFTLCWLPFFIVNIVHVIQDNLIRKEVYILLNWIGYV	317
HRH1_HUMAN	--KAAKQLGFIMAAFILCWIPYFIFFMVIAFCKNCCNEHLHMFTIWLGYI	459
	N7.45 Y7.53	
ADRB2_HUMAN	NSGFNPLIY-CRSPDFRIAFQELLCLRRSSLKAYGNGYSSNGNTGEQSGY	366
HRH1_HUMAN	NSTLNPLIYPLCNENFKKTFKRILHIRS----------	487

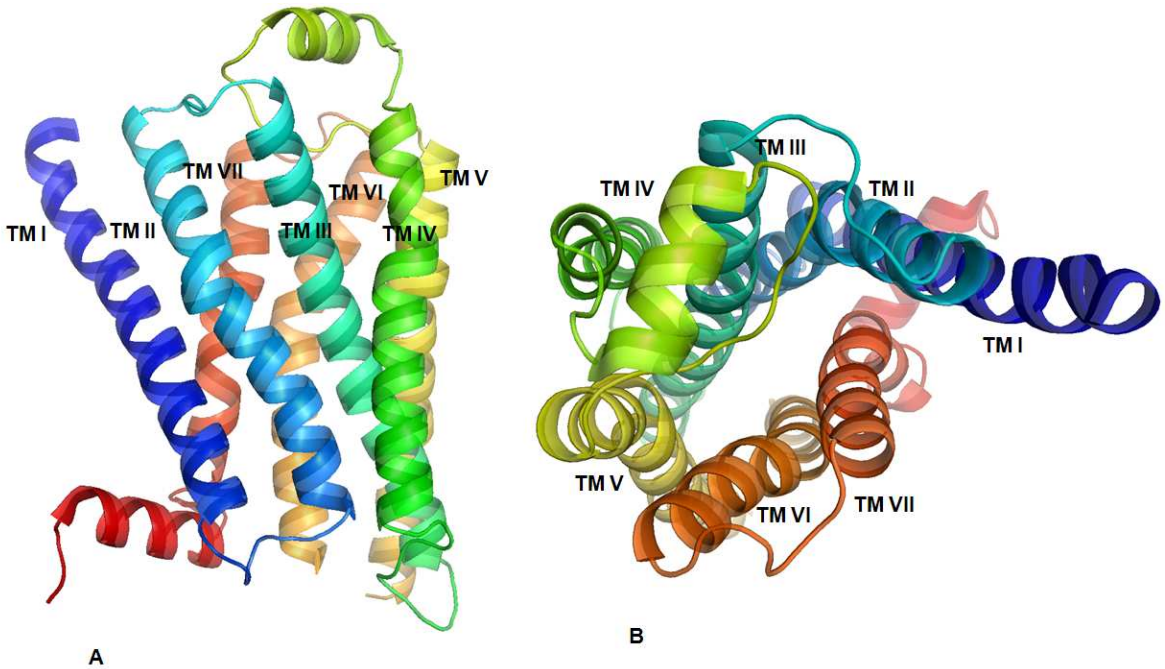

Figure 2. β_2AR-based human H_1 homology model. TM helices are spectrum-color-coded, from blue (TM I) to red (TM VII). Figure was generated with *Pymol* [47]. Left panel: TM bundle oriented with extracellular domains at top and intracellular domains at bottom. Right panel: TM bundle viewed from the extracellular domains down into the receptor cavity

The H_1 homology model in Figure 2 was analyzed using *PDBsum* in *PROCHECK 3.6.2* [48] and resulting statistics are reported in Table 2, while Figure 3 shows the Ramachandran plot. About 87 % of TM residues are in the most favored regions (Psi angle values -180 to 0 degrees) and 13 % are in additional allowed regions (Phi angle values 0 to 180 degrees). No residues were found in generously allowed or in disallowed regions, confirming the structure is acceptable model.

Table 2: Procheck statistics of TM residues in the human H_1 homology model

	Number of residues	%
Most favored regions	221	86.7
Additional allowed regions	33	12.9
Generously allowed regions	0	0

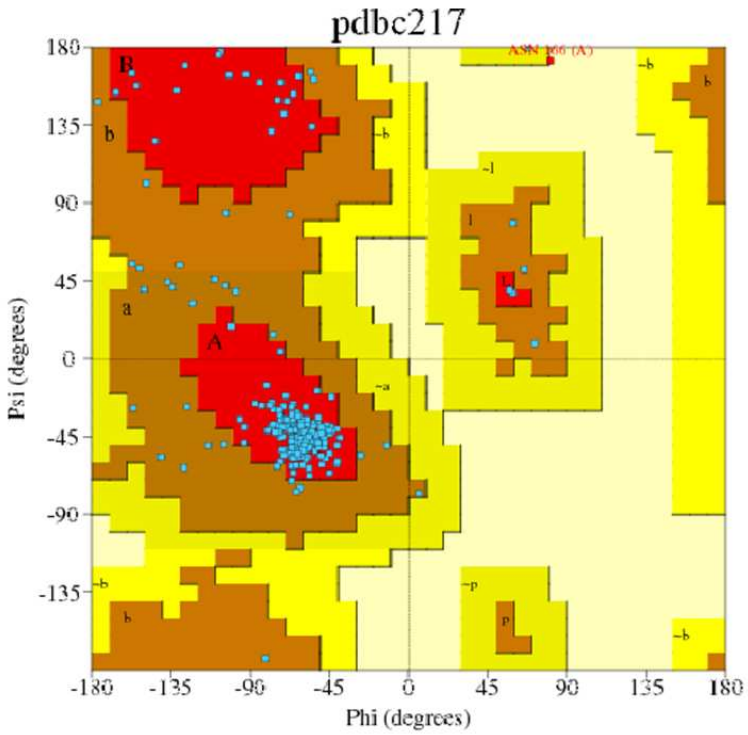

Figure 3. Ramachandran Plot of the human H_1 homology model generated with PROCHECK

A description of the residues contained in each TMH is given in Table 3. The seven TMHs are of variable length (25 - 34 residues), with the longest being TMH III that orients diagonally with respect to the entire TM bundle (Figure 2) and the shortest being TMHs IV and VII (25 residues). TMH VII continues to TMH VIII (12 residues) that orients nearly perpendicular to the TM-spanning bundle (Figure 2).

Table 3: Human H_1 Transmembrane helix (TMH) residues

TMH	Residues in TMH	Reference residue
I	P25-S54, 30 residues	N45 (N1.50)
II	V61-M90, 30 residues	D73 (D2.50)
III	R97-Q130, 34 residues	R124 (R3.50)
IV	K141-W165, 25 residues	W152 (W4.50)
V	T188-H220, 33 residues	P202 (P5.50)
VI	E410-F440, 31 residues	P430 (P6.50)
VII	E447-C471, 25 residues	P465 (P7.50)
VIII	E473-H484, 12 residues	Not applicable

The β_2AR-based human H_1 homology model developed here was compared to our previously reported bRho-based human H_1 homology model [26] (Figure 4). The two structures were superimposed by aligning the alpha carbons in the TM domains and the average distance between superimposed atoms was calculated. The weighted root mean square distance (RMSD) was calculated as 4.49 Å, indicating close similarity of the models [49], however, some differences are apparent due to the two different template receptor structures used. Noteworthy is a slight kink of TMH 1 in the bRho-based model that is not apparent in the β_2AR-based model. Also, TMH V is shorter in the bRho-based model. Overall, however, the TMHs of both models orient in a very similar manner.

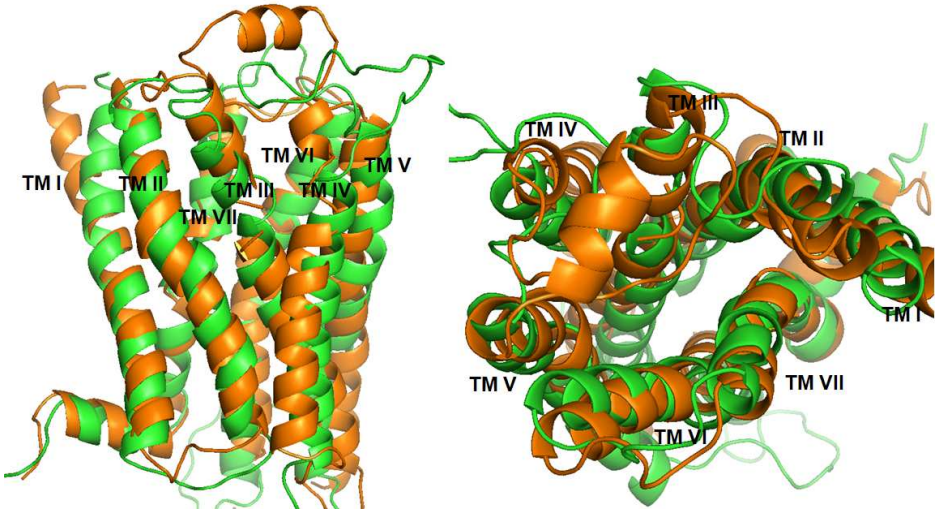

Figure 4. Comparison of the β_2AR-based (orange ribbons) and bRho-based human H_1 homology models. Left panel: TM bundle oriented with extracellular domains at top and intracellular domains at bottom. Right panel: TM bundle viewed from the extracellular domains down into the receptor cavity. Overall RMSD = 4.49 Å

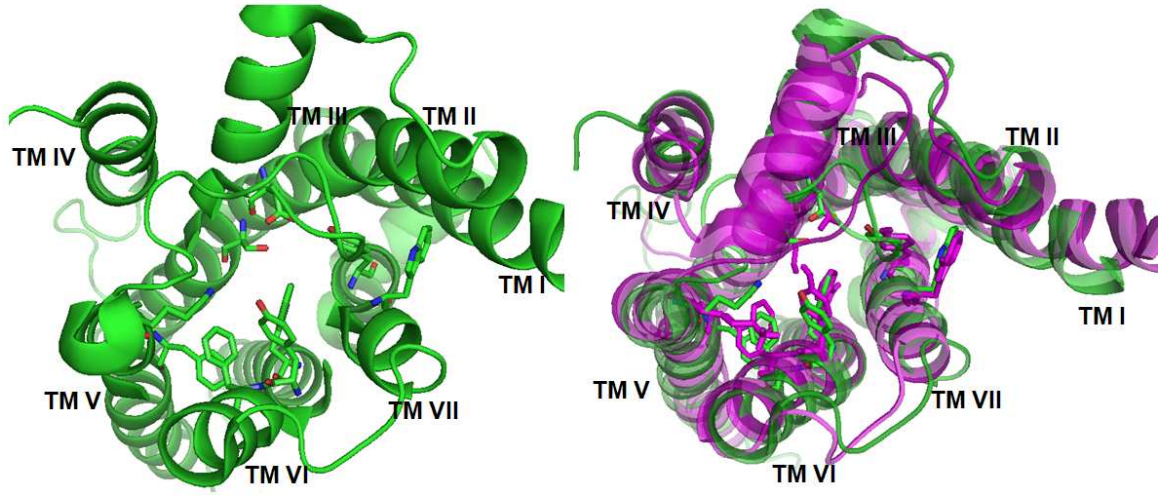

Figure 5. Comparison of 3RZE (green ribbons; for clarity doxepin is not shown) and the β_2AR-based H_1 homology (pink ribbons) models. Left panel: 3RZE oriented with extracellular domains at top and intracellular domains at bottom. Right panel: Superimposition of the β_2AR-based H_1 homology model with 3RZE structure. Conserved residues in the binding pocket are shown. Overall RMSD = 2.91 Å

The β_2AR-based human H_1 homology model developed here also was compared to the recently reported crystal structure of human H_1 receptor in complex with the antagonist doxepin at 3.1 Å resolution, (PDB code 3RZE) [21] (Figure 5). When all alpha carbons of the two structures were aligned, the overall RMSD result was 2.91 Å, indicating the β_2AR-based homology model has very close similarity to the 3RZE structure model. A noteworthy difference between the two structures is that the homology model has a small helix in the extracellular domain (TMH VIII, not shown in Figure 5) that is characteristic of the β_2AR structure template, but which is not present in the 3RZE structure.

Additional comparison of the β_2AR-based H_1 homology and crystal structure (3RZE) models was undertaken by aligning the alpha carbons of binding pocket residues conserved in each of the structures, i.e., D3.32, S3.36, F5.47, W6.48, Y6.51, F6.52, W7.40, and Y7.43 (Figure 6). The RMSD result was 0.597 Å, indicating a very close alignment.

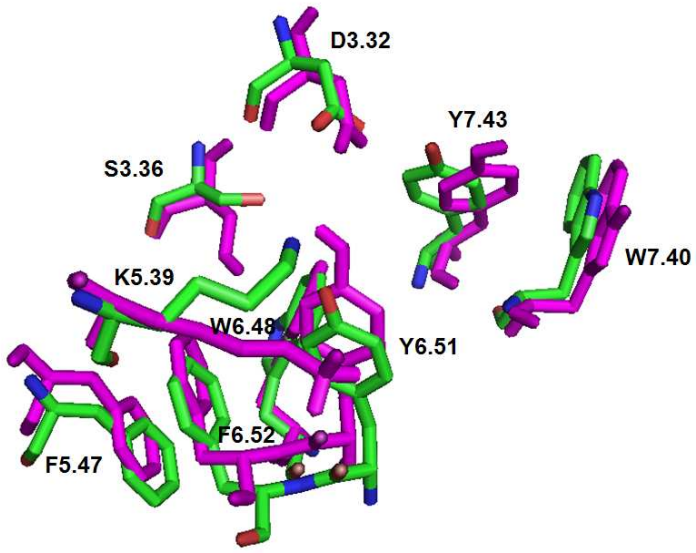

Figure 6. Alpha carbons of conserved residues in the binding pockets of the unbound β_2AR-based H_1 homology (pink) and 3RZE (green) models were aligned and superimposed; RMSD 0.597 Å.

Ligand docking at the β_2AR-based human H_1 homology model

Residues observed in the putative pocket of the β_2AR-based H_1 homology model included, V2.57, N2.61, W3.28, M3.31, D3.32, Y3.33, V3.34, S3.36, T3.37, W4.56, V4.57, F5.38, K5.39, T5.42, A5.43, N5.46, F5.47, W6.48, Y6.51, F6.52, F6.55, H7.35, M7.36, I7.39, W7.40, and Y7.43. With no ligand bound, the H_1 model showed that the carboxylate group of D3.32 interacted with the *para*-hydroxy group of the Y7.43 residue at 3.5 Å distance This D3.32–Y7.43 interaction also was observed recently for the unbound serotonin 5-HT_{2C} GPCR model built by homology to the β_2AR structure [28]. Likewise, in the template β_2AR structure (bound to the inverse agonist carazolol), the same interaction between D3.32 and Y7.43 (3.4 Å) was found [13-15]. It has been proposed that Y7.43 plays a role in stabilizing the negative charge of the D3.32 carboxylate residue in the human H_1, 5-HT_{2C}, and β_2AR GPCRs [27, 28]. In the human H_1 crystal structure with doxepin bound (3RZE), the distance of the D3.32 carboxylate side chain and the Y7.43 *para*-hydroxy group is 1.5 Å, suggesting a very strong interaction.

Figure 7 shows that when histamine was docked at the WT H_1 homology model, the distance between the D3.32 carboxylate moiety and the Y7.43 *para*-hydroxy group decreased from 3.5 Å to 1.5 Å. Thus, it appears that stabilization of the D3.32 carboxylate moiety by the Y7.43 tyrosine moiety is more important in the histamine-bound H_1 receptor compared to the unbound receptor. It would be predicted from the current computational and modeling results that Y7.43 is important for histamine binding and this hypothesis was directly tested experimentally via measurement of histamine binding at the Y7.43A point-mutated human H_1 receptor (see below)—experimental results confirmed *in silico* results.

The protonated ethylamine group of histamine formed a hydrogen bond to the D3.32 carboxylate group (1.9 Å) and also to the S3.36 hydroxyl moiety (2.9 Å). The imidazole ring of histamine docked close to the aromatic ring of Y3.33 (4 Å) and above the aromatic cluster formed by F5.47, W6.48, Y6.51, and F6.52. The histamine imidazole protonated (*tele*) nitrogen (NH) interacted with the *para*-hydroxy of Y3.33 (4.0 Å). No direct interactions were observed between histamine and W4.56 and F5.47, however, interactions with F6.52 (3.5 Å) were possible. It is also noted that F5.47 apparently formed π-π stacking interactions with F6.52. The F6.55 residue, about one helical turn from F6.52, was relatively far away from histamine (6.1 Å). Overall, histamine docked close to TMH V and likely formed electrostatic interactions with residues K5.39, T5.42 and N5.46. For example, the histamine imidazole unprotonated (*pros*) nitrogen docks relatively close (3.1 Å) to K5.39, favorable for hydrogen bonding. Also, the imidazole protonated (*tele*) NH moiety docks close to the OH moiety of T5.42 (4.1 Å) and very close to the carbonyl oxygen of N5.46 (2.6 Å), forming hydrogen bonds.

The results obtained here for histamine interactions with the β_2AR-based human H_1 homology model are consistent with most previous studies that used a bRho-based H_1 homology model [50, 26]. It is noted, however, that one bRho-based human H_1 homology modeling study suggested that histamine docked too far from K5.39 for important hydrogen bonding interactions [51]. However, MD simulations here using the H_1 homology model derived from the β_2AR template indicated that the side chain of K5.39 is able to move closer to histamine upon ligand binding. Moreover, results of experimental studies indicate that affinity of histamine is reduced about 10-times when the human H_1 K5.39 residue is mutated to alanine [26]. In contrast, antagonist H_1 ligands such as mepyramine and (2*S*, 4*R*)-PAT do not bind close to TMH V residues (see Figures 8 and 9, below). Histamine docked to the 3RZE structure model with interactions similar to those described above for docking to the β_2AR-based H_1 homology model (Figure 7). In the histamine-bound 3RZE structure, the distance between the D3.32 carboxylate and Y7.43 *para*-hydroxy groups was 1.5 Å, similar to the β_2AR-based homology model. Specifically, the histamine protonated ethylamine group formed a hydrogen bond to the human H_1 D3.32 carboxylate group (1.8 Å) and the histamine *tele* NH moiety formed a hydrogen bond to the carbonyl oxygen of N5.46 (2.8 Å), as for the homology model. The orientation of the Y3.33 side chain in the 3RZE structure was close to the histamine imidazole moiety and the *pros* (unprotonated) nitrogen could interact with the *para*-hydroxy group of Y3.33 (4.0 Å), essentially the same as for the homology model. Also, as observed in the homology model, residue F6.55 in the 3RZE structure is about one helical turn from F6.52, and consequently far away from the histamine binding pocket. Likewise, residues W4.56 and F5.47 in the 3RZE structure had no direct interactions with histamine (as in the homology model), but, W6.48 was close enough to histamine (3.4 Å) for hydrophobic interactions. Taken together, there were no noteworthy differences regarding histamine–H_1 receptor binding interactions calculated from the H_1 models built by homology to β_2AR and from the human H_1 crystal structure.

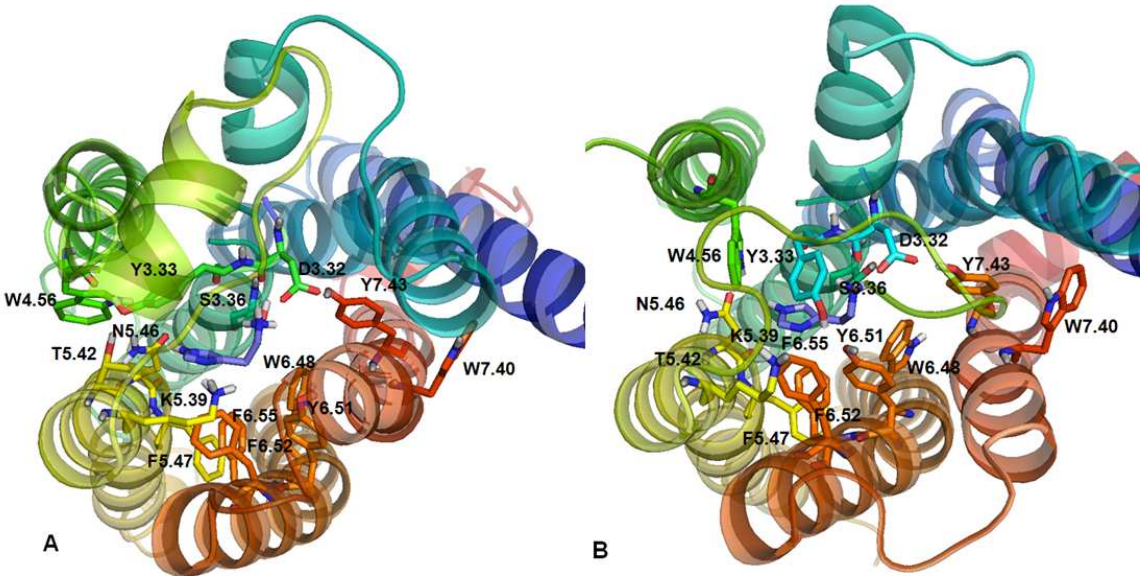

Figure 7. A panel: Histamine docked at β_2AR-based human H_1 receptor homology model. B panel: Histamine docked at the human H_1 crystal structure (3RZE) model

Figure 8 shows mepyramine interactions in the binding pocket of the β_2AR-based H_1 homology model in comparison to the H_1 crystal structure (3RZE) model. The distance between H_1 residues D3.32 and Y7.43 was 2.3 Å in the homology model, similar to the 1.8 Å distance observed in the 3RZE-derived model. Similar to the docking of histamine, the protonated dimethylamine moiety of mepyramine apparently formed a hydrogen bond with the carboxylate side chain of D3.32 at a distance of 1.7 Å in the homology model and 1.5 Å in the 3RZE-derived model. In both the homology and crystal structure H_1 models, mepyramine docked above the aromatic cluster formed by W6.48, Y6.51 and F6.52, with F6.52 also forming π-π stacking interactions with F5.47. No direct interactions were observed between mepyramine and the W4.56 and F6.55 residues, similar to the results for histamine. Upon binding of mepyramine, MD simulations showed the side chain of Y3.33 moves inward toward the binding pocket to form hydrophobic interactions with mepyramine, and the indole ring of W4.56 orients in the contact region between TMHs IV and V.

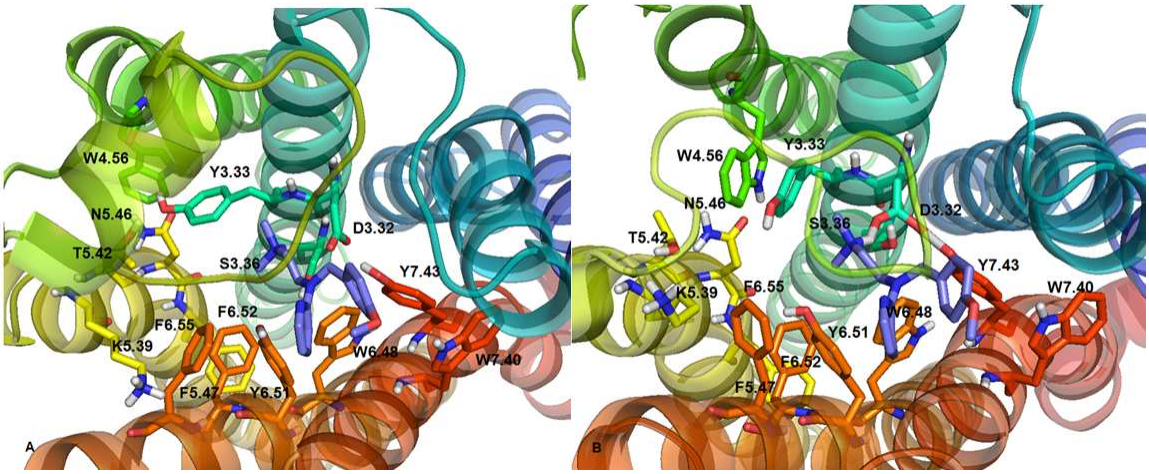

Figure 8. A panel: Mepyramine docked at the β_2AR-based human H_1 receptor homology model. B panel: Mepyramine docket at the human H_1 crystal structure (3RZE) model

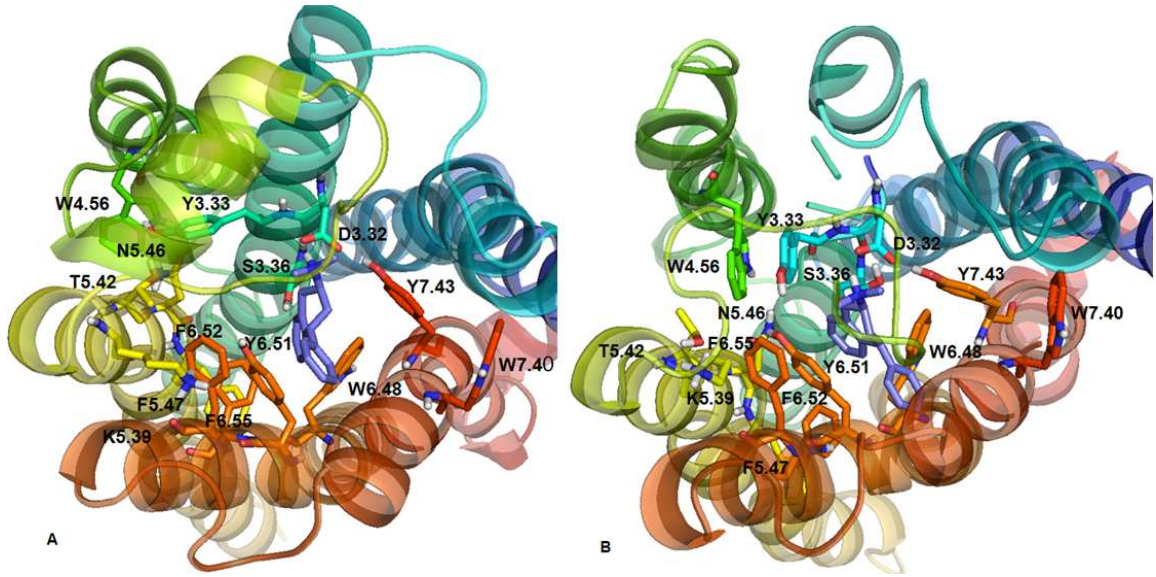

Figure 9. A panel: (2*S*, 4*R*)-PAT docked at β_2AR-based human H_1 receptor homology model. B panel:. (2*S*, 4*R*)-PAT docked at the human H_1 crystal structure (3RZE) model.

Figure 9 shows (2*S*, 4*R*)-PAT interactions in the binding pocket of the β_2AR-based H_1 homology model in comparison to the 3RZE structure model. The interaction between the D3.32 and Y7.43 side chains occurred at 1.9 Å in the homology model and 1.6 Å in the 3RZE model, similar to the interactions observed for histamine and mepyramine. Likewise, the protonated dimethylamine group of (2*S*, 4*R*)-PAT hydrogen bonded to the carboxylate side chain of D3.32 at 1.7 Å distance in both the homology model and 3RZE model, as was the case for histamine and mepyramine. The (2*S*, 4*R*)-PAT tetrahydronaphthalene aromatic ring docked close (3.4 Å) to the indole side chain of W6.48 in the homology model, but, in the 3RZE model, the tetrahydronaphthalene system was closer (4.0 Å) to Y6.51. The 4'-phenyl moiety of (2*S*, 4*R*)-PAT oriented close to W6.48 (4.4 Å) in both the homology and 3RZE models (3.2 and 3.0 Å, respectively). The 4'-phenyl moiety was parallel and relatively close (4.2 Å) to the Y6.51 side chain in the homology model, but far from Y6.51 in the 3RZE model. The *para*-hydroxy group of Y3.33 formed an interaction with the indole –NH of W4.56 and also with the –OH moiety of T5.42. The side chains of F6.52 and F5.47 are near parallel and likely formed π-π stacking interactions (3.8 Å). As was the case for both agonist (histamine) and antagonist (mepyramine) H_1 ligands studied here, the antagonist (2*S*, 4*R*)-PAT did not directly interact with W4.56 and F6.55, but, did interact with the side chain of Y3.33, which moved closer to the binding pocket during MD simulations, as was the case for mepyramine. Also, as is the case for mepyramine, the indole side chain of W4.56 moved during MD simulation to a position between TMHs IV and V. Overall, the H_1

antagonist (2*S*, 4*R*)-PAT oriented similar to the antagonist mepyramine, close to TMH VI and VII, whereas, the agonist histamine docked closer to TMH V.

Ligand binding at WT and point-mutated human H_1 receptors

No specific binding of [^{3}H]-mepyramine or [^{3}H]-(2*S*, 4*R*)-PAT was detected at the D3.32A, Y3.33A, W4.56A, F5.47A, W6.48A, Y6.51A, and F6.52A point-mutated human H_1 receptors—accordingly, histamine affinity also could not be measured at these receptors. Affinity of the H_1 test ligands at WT, F6.55A, and Y7.43A H_1 receptors, however, could be measured and results are summarized in Table 4.

Table 4: Ligand affinity at WT, F6.55A and Y7.43A human H_1 receptors.

Receptor	[^{3}H]-Mepyramine (K_D, nM)	[^{3}H]-(2*S*, 4*R*)- PAT (K_D, nM)	Histamine (K_i)
WT	0.84 ± 0.10	1.47 ± 0.34	3.0 ± 0.3 μM
F6.55A (F435)	4.77 ± 0.88 (P<0.01 vs. WT)	0.39 ± 0.88 (P<0.001 vs. WT)	>1 *m*M
Y7.43A (Y458)	0.87 ± 0.02	1.02 ± 0.14	51 ± 2.1 μM (P<0.001 vs. WT)

The lack of binding for [^{3}H]-mepyramine and [^{3}H]-(2*S*, 4*R*)-PAT binding at D3.32A and F6.52A receptors confirms previous results for the human H_1 GPCR [41]. Furthermore, the current results are consistent with mutagenesis studies of other aminergic GPCRs regarding the D3.32 residue, which has been determined to be essential for ionic bond interaction with the ligand protonated amine moiety [24-26]. Thus, although histamine binding could not be measured here by radioligand displacement, it is expected that histamine does not bind to the D3.32A H_1 receptor. In fact, histamine is not able to activate the D3.32A H_1 receptor regarding PLC-linked intracellular signaling [52]. The lack of binding for the radioligands at the human F6.52A point-mutated H_1 receptor observed here and elsewhere [41] is consistent with results of mutagenesis studies for other aminergic GPCRs phylogenetically related to H_1 (e.g., serotonin 5-HT_{2A}). It appears that the F6.52 residue contributes important and in some cases essential hydrophobic interactions with ligands containing aromatic moieties [53].

The Y3.33A, W4.56A, F5.47A, W6.48A, and Y6.51A point-mutated human H_1 receptors have not previously been reported. The abolished binding for [^{3}H]-mepyramine and [^{3}H]-(2*S*, 4*R*)-PAT observed at the Y3.3A receptor is consistent with the computational results, above. For example, during docking and MD simulations for both ligands at both the WT H_1 β_2AR-based homology and crystal structure (3RZE) models, the Y3.33 side chain rotated toward the binding pocket, likely, contributing to hydrophobic interactions with mepyramine and (2*S*, 4*R*)-PAT (Figures 8 and 9). It is expected that histamine also would have little affinity for the Y3.33A receptor, based on the modeling results above that indicate histamine has substantial binding interactions with Y3.33. For example, for both the WT H_1 homology and 3RZE structure models, the histamine imidazole ring docked close to the aromatic ring of Y3.33 and the imidazole protonated (*tele*) nitrogen (NH) interacted with the *para*-hydroxy moiety of Y3.33 (Figure 7).

The lack of test ligand binding at the W4.56A H_1 receptor is consistent with docking results at the WT H_1 β_2AR-based homology and crystal structure (3RZE) models (Figures 7-9) which indicate no direct interactions between the ligands and receptor. Interestingly, MD simulations showed that the indole side chain of W4.56 positions between TMHs IV and V. Speculatively, the W4.56 residue may contribute to receptor TM bundle packing, which may be compromised by mutation to alanine.

Abolished ligand binding at the F5.47A H_1 receptor is consistent with studies of other aminergic GPCRs, such as, the serotonin 5-HT_{2A} receptor, where the F5.47A point-mutation has significant effects on ligand binding and reduces potency and efficacy of serotonin activation [43, 44]. It is noted that modeling studies showed the F5.47 phenyl side to be nearly parallel to the F6.52 phenyl moiety, apparently, forming π-π interactions that may be critical to stabilization of the binding pocket configuration.

Lack of ligand binding at the W6.48A and Y6.51A H_1 receptors is consistent with the molecular modeling results. Specifically, W6.48 and Y6.51, along with F6.52, form an aromatic cluster that is highly conserved in GPCRs and important for ligand binding [43]. As indicated above (Figures 7 and 8), the aromatic rings of histamine and mepyramine docked close above the aromatic cluster formed by F5.47, W6.48, Y6.51, and F6.52, with apparent π-π stacking interactions formed between with F5.47 and F6.52. For (2*S*, 4*R*)-PAT (Figure 9), the tetrahydronaphtalene

system was close to the W6.48 indole side chain and the pendant 1-phenyl moiety of (2*S*, 4*R*)-PAT oriented parallel to the Y6.51 side chain, presumably engaging in π-π stacking interactions. Taken together, it appears than mutation of any residues of the aromatic cluster formed by F5.47, W6.48, Y6.51, and F6.52 results in loss of critical aromatic ligand binding interactions.

At the F6.55A point-mutated human H_1, histamine had a large (at least 300-times) loss of affinity whereas [^{3}H]-mepyramine had a modest 6-times decreased affinity compared to the WT receptor (Table 4). These results are similar to previously reported results [44]. In contrast to histamine and [^{3}H]-mepyramine, [^{3}H]-(2*S*, 4*R*)-PAT had nearly 4-times *increased* affinity at the F6.55A compared to the WT receptor.

It is noted that both the WT H_1 β_2AR-based homology and crystal structure (3RZE) models (Figure 5) showed that F6.55 is located close to the extracellular domain, one helical turn away from F6.52 and above the aromatic cluster formed by residues F5.47, W6.48, Y6.51, and F6.52. Histamine docked close to TMHs III and V and there were no significant interactions between F6.55 and histamine (Figure 7), which is surprising based on the experimental results indicating a large loss of affinity for histamine at the F6.55A H_1 receptor compared to the WT receptor (Table 4). Previous studies demonstrated histamine agonist potency was reduced about 400-times at the F6.55A compared to WT H_1 receptor [44], a finding consistent with its >300-times reduction of affinity determined here (Table 4). It is also noted that previous studies [44] showed basal signaling activity of the F6.55A H_1 receptor was about 60% less than the WT H_1 receptor, suggesting, the F6.55A point-mutation may change receptor structure, negatively impacting affinity and function of some ligands, but, not others. For example, mepyramine and (2*S*, 4*R*)-PAT docked close to TMHs VI and VII (Figures 8 and 9) and mepyramine likely formed hydrophobic contacts with F6.55, consistent with the experimentally determined 6-times loss of affinity for mepyramine at the F6.55A compared to the WT H_1 receptor (Table 4). In comparison to mepyramine, (2*S*, 4*R*)-PAT docked deeper in the H_1 binding pocket (closer to intracellular region), likely, precluding hydrophobic interactions with F6.55, thus, there was no loss of (2*S*, 4*R*)-PAT affinity when F6.55 was mutated to alanine (in fact, affinity was slightly increased).

At the Y7.43A point-mutated H_1 receptor, affinity of [^{3}H]-mepyramine was not different than at the WT receptor, consistent with previously reported results [54]. Affinity of [^{3}H]-(2*S*, 4*R*)-PAT also was not different at the Y7.43A compared to WT receptors. Affinity of histamine decreased by 17-times at the Y7.43A compared to the WT H_1 receptor (Table 4), which is not in agreement with a previous study [54] where no difference in histamine affinity was observed as the two receptors.

In support of the current results, the Y7.43A point-mutation in the serotonin 5-HT_{2A} receptor, that is phylogenetically closely-related to the H_1 receptor, demonstrated 10-times reduced affinity, 300-times reduced functional potency, and 10-times reduced efficacy of serotonin compared to the WT 5-HT_{2A} receptor [55]. The current experimental results for the 7.43A receptor also are consistent with computational results, above. For example, interaction between the D3.32 and Y7.32 side chains is much closer for the histamine-bound WT H_1 receptor compared to the unbound receptor, suggesting, histamine binding stabilizes the D3.32−Y7.32 interaction. In addition, the protonated ethylamine side chain of histamine apparently formed electrostatic interactions with the *para*-hydroxy-group of Y7.43 (Figure 7). Thus, loss of the D3.32–Y7.43 interaction in the Y7.43A point-mutated receptor would be predicted to negatively impact histamine affinity, consistent with current experimental results (Table 4). Meanwhile, computational results indicate interaction between D3.32 and Y7.43 does not change upon mepyramine binding to the WT receptor and there is only a small change upon (2*S*, 4*R*)-PAT binding. Also, no direct interactions were observed between Y7.43 and mepyramine or (2*S*, 4*R*)-PAT. Thus, loss of the D3.32–Y7.43 interaction in the Y7.43A point-mutated receptor would be predicted to have little impact on affinity of mepyramine and (2*S*, 4*R*)-PAT, consistent with experimental results (Table 4).

CONCLUSION

To the best of our knowledge this is the first study to report the Y3.33A, W4.56A, F5.47A, W6.48A, and Y6.51A point-mutated human H_1 receptors. Experimental results indicated no radioligand binding at these point-mutated mutated receptors, validating predictions made from computational and modeling results, and confirming the importance of these residues for H_1 ligand binding—an instructive new finding with regard to drug design targeting histamine H_1 receptors.

Similar to the β_2AR and 5-HT_{2C} GPCRs [27, 28], the H_1 receptor D3.32 carboxylate residue was determined to be in close proximity to the Y7.43 *para*-hydroxy group indicating likely hydrogen bond formation between these amino acids. Binding of the agonist histamine facilitated an even closer interaction between D3.32 and Y7.43, suggesting, these H_1 amino acids are in involved in agonist ligand–receptor binding pocket stabilization. Also, direct interactions were noted between histamine and both residues, and there was a nearly 20-times loss of affinity for histamine at the Y7.43A point-mutated receptor, confirming this residue is important to stabilize binding of the endogenous agonist. In contrast, the H_1 antagonists mepyramine and (2*S*, 4*R*)-PAT do not facilitate interactions between D3.32 and Y7.43, nor do they form direct interactions with Y7.43, and experimental results confirmed that affinity of the H_1 antagonists was not greatly affected by the Y7.43A mutation. Other differences in the binding modes of the agonist histamine (close to TMH V) compared to the antagonists mepyramine and (2*S*, 4*R*)-PAT (closer to TMHs VI and VII) support theoretical and experimental studies on GPCRs that conclude ligands can bind differently to stabilize different conformational states of the same GPCR, leading to different functional outcomes [29, 56, 57, 58], of paramount importance in rational drug design and development.

MD simulations here using the H_1 homology model derived from the β_2AR template indicated that the side chain of K5.39 is able to move closer to histamine upon ligand binding. Moreover, results of experimental studies indicate that affinity of histamine is reduced about 10-times when the human H_1 K5.39 residue is mutated to alanine [51]. In contrast, antagonist H_1 ligands such as mepyramine and (2*S*, 4*R*)-PAT do not bind close to TMH V residues (see Figures 8 and 9, below).

Homology models and docking methods have been used to help understand drug- receptor interactions, and drug design, in the absence of crystal structure of the target receptor [27, 28, 59-62]. In the present work, the human H_1 GPCR homology model built from the human β_2AR crystal structure was tested using computational techniques and ligand docking results were validated by experimental binding results using WT and point-mutated human H_1 receptors. The overall structure of the β_2AR-derived model was similar to the previously reported bRho-based human H_1 homology model [26]. The β_2AR-derived H_1 model also was compared to a model built from the crystal structure of the human H_1 receptor in complex with the antagonist doxepin at 3 Å resolution (PDB code 3RZE); the resulting RMSD value was 2.91 Å, close to the resolution of 3RZE. Thus, it is concluded that the human β_2AR is a suitable template for GPCR homology modeling. A similar conclusion was reached regarding β_2AR-based homology and crystal structure models for the dopamine D_3 aminergic GPCR [63]. Indeed, it recently was suggested that carefully built homology-based GPCR models may be more practical for structure-based drug design because they can capture subtle but critical chemical and structural features of the binding pocket that are not necessarily obvious from X-ray crystal structures [64]. Likewise, results here indicated there were no noteworthy differences regarding ligand–H_1 receptor binding interactions calculated from the H_1 models built by homology to β_2AR and from the human H_1 crystal structure, indicating, the homology-derived model could continue to be a suitable template for H_1 receptor drug design.

Acknowledgement
This work was supported by National Institutes of Health grants DA023928, DA030989, MH081193.

REFERENCES

[1] JC Schwartz, JM Arrang, M Garbarg, H Pollard, M Ruat, *Physiol. Rev*. **1991**, 71, 1-51.
[2] JS Hill, *Pharmacol. Rev*. **1990**, 42, 45-83, SJ Hill, CR Ganellin, H Timmerman, JC Schwart, NP Shankley, JM Young, W Schunack, R Levi, HL Haas, *Pharmacol. Rev*. **1997**, 49, 253-278.
[3] NY Choksi, WB Nix, SD Wyrick, RG Booth, *Brain Res*. **2000**, 852, 151-160.
[4] K Palczewski, T Kumasaka, T Hori, CA Behnke, H Motoshima, BA Fox, I Le Trong, DC Teller, T Okada, RE Stenkamp, M Yamamoto, M Miyano, *Science*. **2000**, 289, 793-745.
[5] J Li, PC Edwards, M Burghammer, C Villa, GF Schertler, *J. Mol. Biol*. **2004**, 343(5), 1409-1438.
[6] T Okada, M Sugihara, AN Bondar, M Elstner, P Entel, V Buss, *J. Mol. Biol*. **2004**, 342(2), 571-583.
[7] T Okada, Y Fujiyoshi, M Silow, J Navarro, EM Landau, Y Shichida, *Proc. Natl. Acad. Sci*. U.S.A., **2002**, 99, 5982-5987.
[8] DC Teller, T Okada, CA Behnke, K Palczewski, RE Stenkamp, *Biochemistry*. **2001**, 40 (26), 7761-7772.
[9] JH Park, P Scheerer, KP Hofmann, HW Choe, OP Ernst, *Nature*. **2008**, 454, 183-187.
[10] P Scheerer, JH Park, PW Hildebrand, YJ Kim, N Krauβ, HW Choe, KP Hofmann, OP Ernst, *Nature*. **2008**, 455, 497-502.

[11] VP Jaakola, MT Griffith, MA Hanson, V Cherezov, EYT Chien, JR Lane, AP Ijzerman, RC Stevens, *Science*. **2008**, 322, 1211-1217.
[12] T Warne, MJ Serrano-Vega, JG Baker, R Moukhametzianov, PC Edwards, R Henderson, AGW Leslie, CG Tate, GFX Schertler, *Nature*. **2008**, 454, 486-491.
[13] V Cherezov, DM Rosenbaum, MA Hanson, SGF Rasmussen, FS Thian, TS Kobilka, HJ Choi, P Kuhn, WI Weis, KB Kobilka, RC Stevens, *Science*. **2007**, 318, 1258-1265.
[14] MA Hanson, V Cherezov, MT Griffith, CB Roth, VP Jaakola, EY Chien, J Velasquez, P Kuhn, RC Stevens, *Structure*. **2008**, 16, 897-905.
[15] SG Rasmussen, HJ Choi, DM Rosenbaum, TS Kobilka, FS Thian, PC Edwards, M Burghammer, VRP Ratnala, R Sanishvili, RF Fischetti, GFX Schertler, WI Weis, BK Kobilka, *Nature*. **2007**, 450**,** 383-387.
[16] DM Rosenbaum, V Cherezov, MA Hanson, SGF Rasmussen, FS Thian, TS Kobilka HJ Choi, XJ Yao, WI Weis, RC Stevens, BK Kobilka, *Science*. **2007**, 318, 1266-1273.
[17] SG Rassmussen, HJ Choi, JJ Fung, E Pardon, P Casarosa, PS Chae, BT DeVree, DM Rosembaum, FS Thian, TS Kobilka, A Schnapp, I Konetzki, RK Sunahara, SH Gellman, A Pautsch, J Steyaert, WI Weis, BK Kobilka, *Nature*. **2011**, 469, 175-181.
[18] DM Rosembaum, C Zhang, JA Lyons, R Holl, D Aragao, DH Arlow, SG Rasmussen, HJ Choi, BT DeVree, RK Sunahara, PS Chae, SH Gellman, RO Dror, DE Shaw, WI Weis, M Caffrey, P Gmeiner, BK Kobilka, *Nature*. **2011**, 469, 236-240.
[19] M Congreve, CJ Langmea, JS Mason, FH Marshall, *J. Med. Chem.* 2011, 54(13), 4283-4311.
[20] E.Y.T Chien, W. Liu, Q. Zhao, V. Katritch, G.W. Han, M.A. Hanson, L. Shi, A.H. Newman, J.A. Javitch, V. Cherezov, R.C. Stevens, R.C. *Science*, **2010**, 330(6007), 1091-1095.
[21] T Schimamura, M Shiroishi, S Weyand, H Tsujimoto, G Winter, V Katritch, R Abagyan, V Cherezov, W Liu, GWon Han, T Kobayashi, RC Stevens, S Iwata, *Nature*. **2011**, 475, 65-70.
[22] RG Booth, L Fang, Y Huang, A Wilczynski, S Sivendran, *Eur. J. Pharmacol*. **2009**, 615**,** 1-9.
[23] EC Bucholtz, RL Brown, A Tropsha, RG Booth, SD Wyrick, *J. Med. Chem.* **1999**, 42, 3041-3054.
[24] K Kristiansen, SG Dahl, *Eur. J. Pharmacol*. **1996**, 306**,** 195-210.
[25] K Kristiansen, WK Kroeze, DL Willins, EI Gelber, JE Savage, RA Glennon, BL Roth, *J. Pharmacol. Exp. Ther*. **2000**, 293**,** 735-746.
[26] RG Booth, L Fang, A Wilczynski, S Sivendren, Z Sun, S Travers, M Bruysters, K Sansuk, R Leurs, *Inflam. Res*, **2008**, 57, suppl 1, S43-S44.
[27] C Canal, TC Cordova-Sintjago, NY Villa, LJ Fang, RG Booth, *Eur. J. Pharmacol*, **2011**, 673, 1-12.
[28] T Cordova-Sintjago, N Villa, C Canal, R Booth, *Int. J. Quant. Chem*. **201**1, 112, 140-149
[29] NH Moniri, D Covington-Strachan, RG Booth, *J. Pharmacol. Exp. Ther*. **2004**, 311(1), 274-81
[30] JD Thompson, DG Higgins, TJ Gibson, *Nucleic Acids Res*. **1994**, 22(22):4673-4680.
[31] MA Larkin, G Blackshields, NP Brown, R Chenna, PA McGettigan, H McWilliam, F Valentin, IM Wallace, A Wilm, R Lopez, JDThompson, TJ Gibson, DG Higgins, *Bioinformatics*, **2007**, 23**,** 2947-2948.
[32] *SYBYL* 8.0, Tripos International, 1699 South Hanley Rd., St. Louis, Missouri, 63144. USA
[33] M Clark, RD III Cramer, N van Opdenhosch, *J. Comp. Chem*. **1989**, 10, 982-1012.
[34] WD Cornell, P Cieplak, CI Bayly, IR Gould, KM Jr Merz, DM Ferguson, DC Spellmeyer, T Fox, JW Caldwell, PA Kollman, *J. Am. Chem. Soc*. **1995**, 117, 5179–5197.
[35] H Heller, M Schaefer, K Schulten, *J. Phys. Chem*. **1993**, 97**,** 8343-8360.
[36] SD Wyrick, AM Myers, RG Booth, NS Kula, RJ Baldessarini, RB Mailman, *J. Labeled Comp Radiopharm*. **1994**, 34: 131-134
[37] *HyperChem* (TM) Professional 8.0, Hypercube, Inc., 1115 NW 4th Street, Gainesville, Florida 32601, USA
[38] D Schneidman-Duhovny, Y Inbar, R Nussinov, HJ Wolfson, *Nucl. Acids. Res*. **2005**, 33, W363-367.
[39] J Gasteiger, M Marsili, *Tetrahedrom*. **1980**, 36, 3219-3288.
[40] LA Goldman, EC Cutone, SV Kotenko, CD Krause, *Biotechnique*s. **1996,** 21(6), 1013-1015.
[41] RA Bakker, G Dees, JJ Carrillo, RG Booth, JF López-Gimenez, G Milligan, PG Strange, R Leurs, *J Pharmacol Exp The*r. 2004 Oct;311(1):131-8.
[42] M Bruysters HH Pertz, A Teunissen RA Bakker, M Gillard, P Chatelain P, *Eur J Pharmacol.* 2004; 487:55–63.
[43] DA.Shapiro, K Kristiansen, WK Kroeze, BL Roth, *Mol. Pharmacol.* **2000**, *58*, 877-886
[44] M Bruysters, HH Pertz, A Teunissen, RA Bakker, M Gillard, P Chatelain, *Eur J Pharmacol*. **2004**; 487,55–63
[45] Y Cheng, WH Prusoff, *Biochem Pharmacol*. **1973**, 22, 3099-3108
[46] a JA Ballesteros, AD Jensen, G Liapakis, SGF Rasmussen, L Shi, U Gether, JA Javitch, *J. Biol. Chem*.**2001**, 276(31)**,** 29171-29177.; b. JA Ballesteros, L Shi, JA Javitch, *Mol. Pharmacol*. **2001**, 60(1)**,** 1-19.

[47] WL Delano, the PyMOL Molecular Graphics System, Version 1.3, Schrödinger, LLC, www.pymol.org/citing
[48] RA Laskowski, MW MacArthur, DS Moss, JM Thornton, *J. App. Cryst*. **1993**, 26, 283-291.
[49] EA Coultsias, C Seok, KA Dill, *J. Comp. Chem.*, 2004, 25, 1849-1857.
[50] M Gillard, C Van der Perren, N Moguilevsky, R Massingham, P Chatelain, *Mol. Pharmacol*. **2002**, 61(2), 391, 399
[51] R Kiss, Z Kovari, GM Keseru, *Eur. J. Med. Chem.* **2004**, 39, 959-967
[52] K Ohta, H Hayashi, H Mizuguchi, H Kagamiyama, K Fujimoto, H Fukui, *Biochem Biophys Res Commun*. **1994**, 203(2):1096-10
[53] WK Kroeze, K Kristiansen, BL Roth, *Curr Top Med Chem*. **2002**, 2(6):507-28.
[54] M Bruysters, A Jongejan, M Gillard, F van de Manakker, RA Bakker, P Chatelain, R Leurs, *Mol. Pharmacol*. **2005**, 67(4), 1045-1052.
[55] BL Roth, M Shoham, MS Choudhary, N Khan, *Mol. Pharmacol*. **1997**, 52, 259-266.
[56] JD Urban, WP Clarke, M von Zastrow, DE Nichols, B Kobilka, H Weinstein, JA Javitch, BL Roth, A Christopoulos, PM Sexton, KJ Miller, M Spedding, RB Mailman, *J. Pharmacol. Exp. Ther*. **2007**, 320, 1-13
[57] S Bhattacharya, SE. Hall, N. Vaidehi, *Biophys J*. **2008**, 94(6), 2027-2042
[58] TP Kenakin, *Br.J. Pharmacol*, **2011**, 165(6), 1659-1669
[59] P Shankaracharya, AS Vidyarthi, *J.Chem. Pharm. Res*. **2010**, 2(3), 329-337
[60] RK Prasad, R Sharma, GL Prajapati, *J.Chem.Pharm.Res*, **2010**, 2(2), 440-451
[61] MKA Khan, S Akhtar, MH Siddiqui, OA Al-Sagair, JM Arif, *J.Chem.Pharm.Res*, **2011**, 3(1) 756-763
[62] R Gussio, MJ Currens, DA Scudiero, JA Smith, DA Lannigan, RH Shoemaker, DW Zaharevitz, TL Nguyen, *J.Chem.Pharm.Res*, **2010**, 2(5), 587-598
[63] J Carlsson, RG Coleman, V Setola, JJ Irwin, H Fan, A Schlessinger, A Sali, BL Roth, BK Schoichet, *Nature Chemical Biology*, **2011**, 7, 769-778
[64] H Tang, XS Wang, J-H. Hsieh, A Tropsha, *Prot. Struct. Func.Bioifo*, **2012**, 80(6), 1503-1521